Check for updates

ChemPhotoChem

Research Article
doi.org/10.1002/cptc.202400235

Chemistry Europe
European Chemical Societies Publishing

www.chemphotochem.org

Fluorene vs. Spirobifluorene: Effect of the π-System on TADF Properties

Tim Silies,[a] Nikos L. Doltsinis,[b] Constantin G. Daniliuc,[c] and Fabio Rizzo*[a, d]

There are many options to design a molecular structure that could result in thermally activated delayed fluorescence (TADF). One promising strategy is to use the donor-π-acceptor motive where an electron-donating unit is linked to an electron-acceptor via an aryl moiety like phenyl. While this approach is widely used and well understood, the performance of the chromophores can be limited by different energy loss pathways, e.g. internal conversion, or by π-stacking. To circumvent these problems rigid structures with sterically demanding substituents are applied. In this work, we designed two TADF emitters based on phenothiazine and nitrile linked via spiro-9,9′-bi-[fluorene] or 9,9-dimethylfluorene and compared the effect of the linker on the physical properties of the dyes. This work emphasizes the importance of careful design of conjugated spacer for efficient TADF emitters.

Introduction

Thermally activated delayed fluorescence (TADF) materials found use in plenty research fields like organic light emitting diodes,[1] organic photovoltaic cells,[2] bio-, chemo- and photosensors,[3] organic lasers and photocatalysis[4] due to their ability to achieve up to 100% internal quantum conversion without the use of heavy metals.[5] This effect arises from the up-conversion of triplet state to singlet-excited state through reverse intersystem crossing (RISC) process occurring either upon photoexcitation and subsequent intersystem crossing (ISC) (in solution), or upon charge injection (in devices). RISC requires a small singlet-triplet energy gap (ΔE_{ST}) that can be modulated through a suitable molecular design involving linked donor–acceptor (D–A) units spatially separating the highest occupied molecular orbital (HOMO) and lowest unoccupied molecular orbital (LUMO) resulting into intramolecular charge transfer (ICT).[1a,6] Common D motives are nitrogen-containing polyaromatic systems like carbazole, diphenylamine, phenoxazine and other derivatives due to their strong electron-donating ability, stability and high triplet states. As acceptor groups, choices are more divers ranging from cyano-based groups to hetero atom containing or linked aromatic systems.[1a,c,7] Though popular, this molecular design often results in reduced quantum yields in solid state caused by π–π assembly inducing aggregation caused quenching phenomenon.[8] A strategy to counteract this issue is to insert bulky spiro-9,9′-bi[fluorene] (SBF) either as π-system or as sidegroup.[7,9] The perpendicular arrangement of the aromatic core results in a high steric demand with a rigid structure that limits π–π assembly, characteristics allowing the use of SBF in different applications.[10] The cross-shape configuration also leads to better thermal stability and higher glass transition temperatures compared to analogous fluorene derivatives,[11] which are suffering from oxidation on the carbon in position 9 degrading to fluorenone. For this reason, most TADF emitters based on fluorene are designed to display through space ICT,[12] whereas D–A 2,7-substituted fluorene derivatives rarely display TADF behavior.[13] Noteworthy, examples employing nitrile as acceptor in position 7 and phenoxazine[14] or triphenylamine[15] in position 2 as donor are not showing TADF emission, but emission from hybridized local and charge transfer (HLCT) states.[16] Aimed to explore further the use of fluorene derivatives 2,7-substituted as TADF emitters, we prepared and investigated a new derivative (**2**) bearing phenothiazine and nitrile groups as D–A pair, which surprisingly shows TADF emission. Besides, we compared the data with the analogous spirobifluorene derivative (**1**) to get more insights on the influence of the different π-systems on the TADF properties.[14–17]

[a] *T. Silies, F. Rizzo*
Center for Soft Nanoscience (SoN), University of Münster,Busso-Peus-Str. 10, 48149 Münster, Germany

[b] *N. L. Doltsinis*
Institute for Solid State Theory, University of Münster,Wilhelm-Klemm-Str. 10, 48149 Münster, Germany

[c] *C. G. Daniliuc*
Organic Chemistry Institute, University of Münster,Corrensstr. 36, 48149 Münster, Germany

[d] *F. Rizzo*
Institute of Chemical Sciences and Technologies "G. Natta" (SCITEC), National Research Council (CNR),via G. Fantoli 16/15, 20138 Milano, Italy
E-mail: fabio.rizzo@cnr.it

Supporting information for this article is available on the WWW under https://doi.org/10.1002/cptc.202400235

© 2024 The Author(s). ChemPhotoChem published by Wiley-VCH GmbH. This is an open access article under the terms of the Creative Commons Attribution Non-Commercial License, which permits use, distribution and reproduction in any medium, provided the original work is properly cited and is not used for commercial purposes.

© 2024 The Author(s). ChemPhotoChem published by Wiley-VCH GmbH

Results and Discussion

Synthesis

Both chromophores (Figure 1) have been synthesized by following a similar approach as reported in Scheme S1. In **1**, the acceptor was first introduced by palladium catalyzed nitrilation of the corresponding brominated precursor. In the case of the fluorene compound, the nitrilation was carried out on the monobrominated derivative in order to reduce the formation of side-products, followed by bromination using 1,3-dibromo-5,5-dimethylhydantoin (DBDMH) in hexafluoro-2-propanol (HFIP) to give the desired disubstituted intermediate.[18] Afterwards, in both dyes the donor unit was inserted by Buchwald-Hartwig cross coupling using phenothiazine in combination with $Pd(OAc)_2$ and P^tBu_3 as catalyst, giving **1** and **2** in good yields. The compounds were characterized by ^{1}H-NMR, ^{13}C-NMR, HRMS and X-Ray crystallography. Further details of the synthetic procedures are given in the Supporting Information.

Photophysical Studies

The absorption and steady-state photoluminescence (PL) of **1** and **2** measured in toluene at room temperature are shown in Figure 2a. The concentrations were $1.5\cdot10^{-5}$ M and $7\cdot10^{-6}$ M, respectively. Both dyes show a weak absorption band between 335 nm and 380 nm with a tail extending beyond 400 nm, arising from intramolecular charge-transfer (ICT).[19] This assumption appears clear by comparing the absorption spectra of isolated D (phenothiazine) and A (fluorenecarbonitrile) units with dye **2**, showing that the tail beyond 400 nm is compatible with the presence of a new CT band (Figure S2). Intense absorption bands appearing between 290 nm and 335 nm can be assigned to the $S_0\rightarrow_1(\pi-\pi^*)$ transition of the spirobifluorene- and fluorene-cores (Figures S3 and S4). The highly similar absorption curves suggest a negligible effect of the spiro-core on the absorption of the dye. PL spectra of **1** and **2** show main emission in the blue-green region with maximum at 515 nm and 502 nm, respectively. Interestingly, a high energy band is visible in both compounds around 400 nm, which is attributed to the singlet excited state of the quasi-axial conformer of the phenothiazine unit, as reported in literature for other TADF emitters bearing phenothiazine as donor.[16] The main emission band of both dyes with a full-width-at-half-maximum (FWHM) of 89 nm (0.40 eV) and 92 nm (0.44 eV) for **1** and **2**, respectively, can be attributed to the radiative decay from the singlet excited

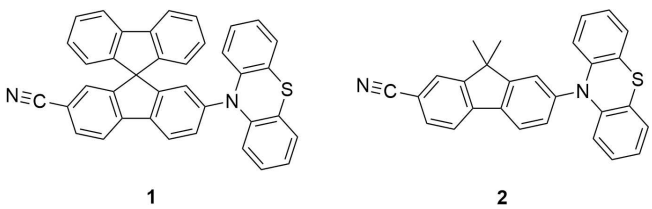

1 **2**

Figure 1. Chemical structures of **1** and **2**.

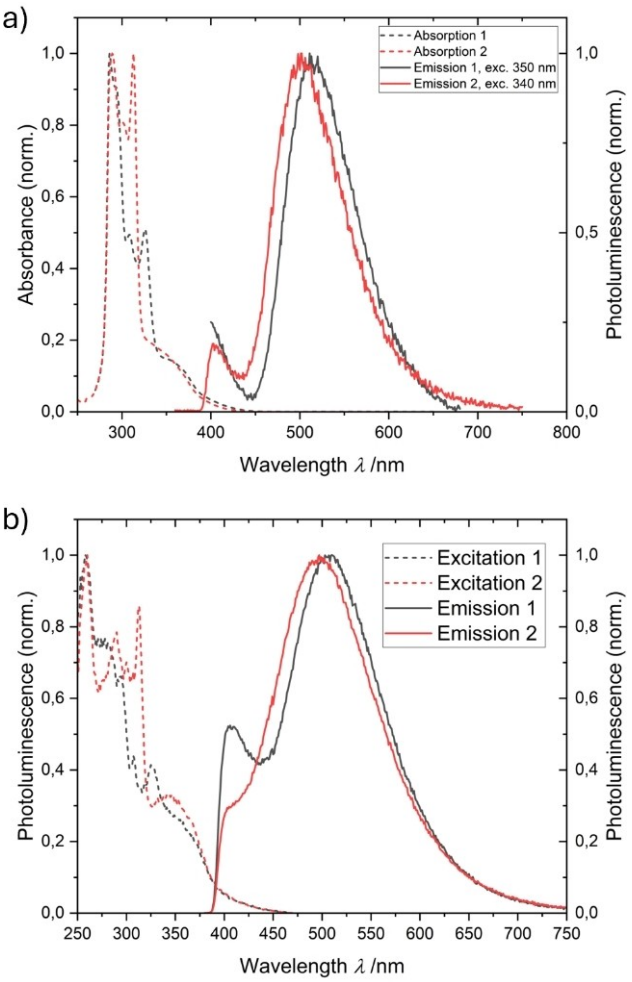

Figure 2. (a) Normalized absorption (dotted lines) and PL (solid lines) spectra of **1** (black color) and **2** (red color) in toluene ($1.5\cdot10^{-5}$ M and $7\cdot10^{-6}$ M for **1** and **2**, respectively); (b) excitation and PL spectra of doped PMMA thin films (10 wt%) of **1** and **2**. A longpass filter for the emission and excitation spectra was used to cut off light below 400 nm.

state of the D–A dye with the quasi-equatorial conformer of phenothiazine. The CT character of the transition is also highlighted by the solvatochromism observed in solution (Figure S5). Figure 2b shows excitation and emission spectra of **1** and **2** in doped PMMA thin film (10 wt%), which was obtained by depositing the corresponding dye-PMMA solution in chloroform onto quartz substrates via spin coating. The excitation spectra of both compounds appear similar to the absorption spectra in toluene, and the low energy ICT absorption band can be better visualized. Compared to solution, the emission peak of **1** is broader with FWHM of 117 nm (0.56 eV) and 5 nm (0.02 eV) blue shifted. Similar to **1**, the emission band of **2** in PMMA is broader (FWHM of 124 nm, 0.62 eV), but larger hypsochromically shifted to 488 nm. It is worth to emphasize the occurrence of the emission band assigned to the quasi-axial conformer of phenothiazine also in thin film for both dyes, even if in **2** the high energy peak appears as shoulder at 403 nm due to the broad quasi-equatorial conformer emission. The observed blue shift in thin films could arise presumably from the

© 2024 The Author(s). ChemPhotoChem published by Wiley-VCH GmbH

23670932, 0, Downloaded from https://chemistry-europe.onlinelibrary.wiley.com/doi/10.1002/cptc.202400235 by Universita'Degli Studi Di Mila, Wiley Online Library on [06/12/2024]. See the Terms and Conditions (https://onlinelibrary.wiley.com/terms-and-conditions) on Wiley Online Library for rules of use; OA articles are governed by the applicable Creative Commons License

low polarity of the surrounding medium affecting the ICT character of **1** and **2**.[20]

To understand the nature of radiative mechanism involves in the recorded emissions, lifetime measurements (Figure 3) of **1** and **2** were carried out in air saturated and degassed toluene solution as well as in thin films (Figures S6–S8). In toluene the radiative decays are mono exponential with typical fluorescence lifetimes (2.8 ns and 2.2 ns for **1** and **2**, respectively). The effect of oxygen appears negligible for both compounds, with a marginal difference on lifetimes, even if a slightly increase on PL intensity upon purging the solution with argon was observed (Figures S6b and S7b). Due to the lack of long component in lifetime and the limited effect of the oxygen on the emission, we can conclude that both dyes do not exhibit TADF in solution. In contrast, lifetime measurements performed in thin films show very long radiative decay in both dyes. **1** and

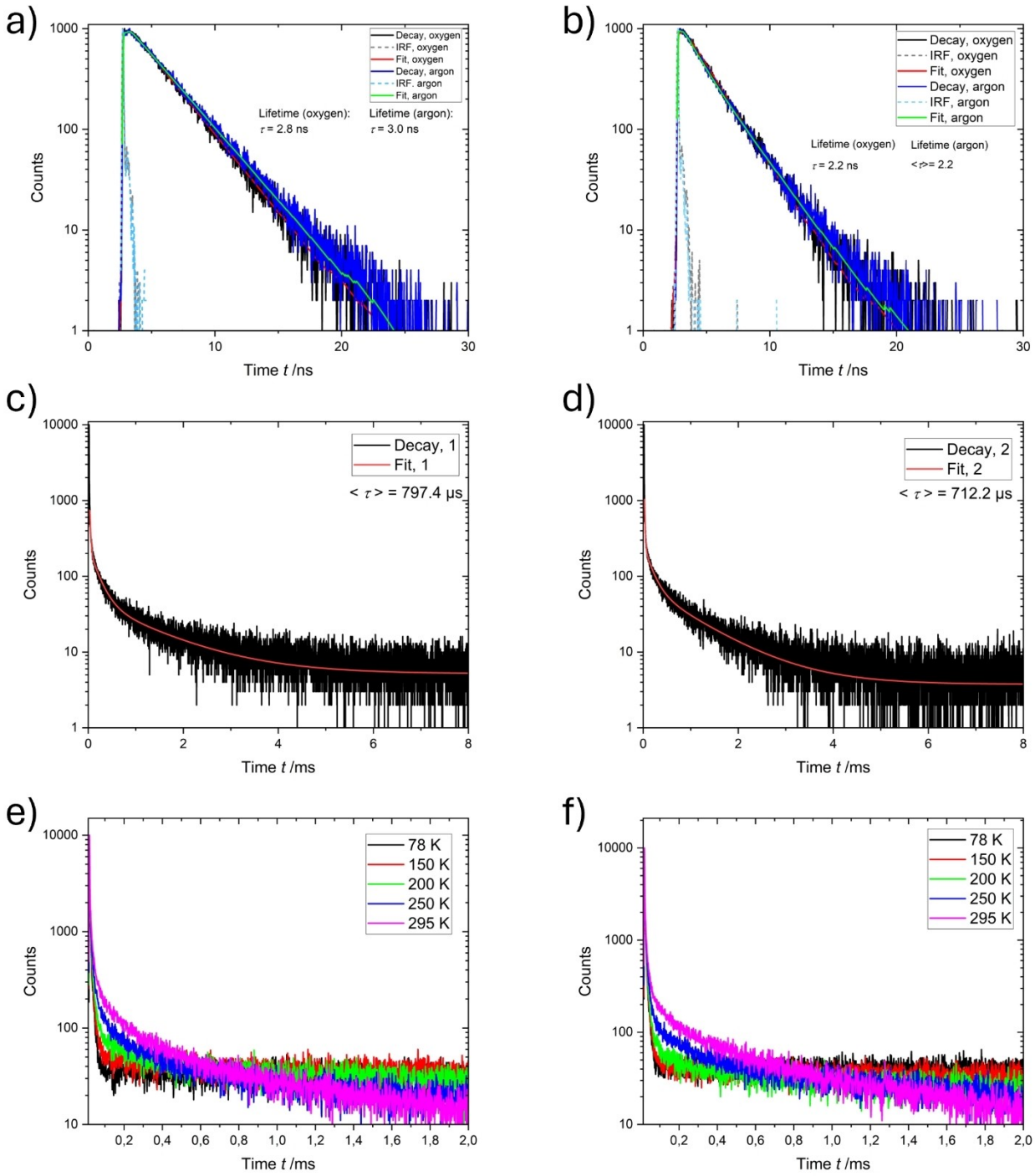

Figure 3. Fluorescence lifetime of **1** (a) and **2** (b) in air saturated and degassed toluene. $\lambda_{exc}=375$ nm, $\lambda_{em}=515$ nm (**1**) and 500 nm (**2**), $c=1.5\cdot10^{-5}$ M (**1**) and $7\cdot10^{-6}$ M (**2**). Fluorescence lifetime of **1** (c) and **2** (d) in doped PMMA thin film (10 wt%) at RT and at different temperatures (e, f). $\lambda_{exc}=350$ nm, $\lambda_{em}=510$ nm (**1**) and 500 nm (**2**). The multiexponential values of the lifetime fit are given in the Supporting Information.

© 2024 The Author(s). ChemPhotoChem published by Wiley-VCH GmbH

23670932, 0, Downloaded from https://chemistry-europe.onlinelibrary.wiley.com/doi/10.1002/cptc.202400235 by Universita'Degli Studi Di Mila, Wiley Online Library on [06/12/2024]. See the Terms and Conditions (https://onlinelibrary.wiley.com/terms-and-conditions) on Wiley Online Library for rules of use; OA articles are governed by the applicable Creative Commons License

2 emissions exhibit a lifetime with prompt fluorescence of 5.5 ns and 4.5 ns and delayed fluorescence component of 797.43 μs and 712.23 μs. Measurements of lifetime carried out at different temperatures (Figure 3e and 3f) allow assigning the radiative decay mechanism as TADF in both compounds. The presence of the long radiative component is very surprising in fluorene derivative, because studies performed on very similar dye bearing phenoxazine and nitrile as D–A pair excluded the occurrence of TADF phenomenon.[14] The photoluminescence quantum yield (PLQY) in doped PMMA thin film (10 wt%) was 9% and 4% for **1** and **2**, respectively. The difference in PLQY could be explained by the lower singlet-triplet energy gap, the decrease in aggregation and the increased rigidity of the SBF scaffold.[9a,21] Noteworthy, gated emission spectra recorded with different delay time show that the quasi-axial conformer in both cases does not contribute to the TADF emission, since the small emission band between 400 nm and 420 nm cannot be observed after 10 μs (Figures S9 and S10). To verify that the polarity is not the cause of the different behavior observed in solution and thin films, we investigated the fluorescence of **1** in ethyl acetate[22] without observing TADF emission (Figure S11).

In addition to toluene solution and doped PMMA thin films, we investigated the photophysical properties of both dyes as crystals (Figures S12–S14). Compared to solution and solid state, crystals grown from dichloromethane (**1**) or toluene (**2**) exhibit emission largely blue-shifted and an intense ICT excitation band due to the non-polar and highly ordered environment (Figures S12c and S13c). Notably, the emission band of the quasi-axial conformer is missing for **1** or negligible for **2**, indicating that the quasi-equatorial conformer is present as main emitting species. As observed in thin film, emission lifetime shows two component radiative decays, with prompt fluorescence of 1.95 ns and 1.67 ns and delayed fluorescence component of 248.64 μs and 153.34 μs for **1** and **2**, respectively, thus shorter compared to the PMMA thin films. The difference of lifetime values between the chromophores can be attribute to the presence of the second fluorene half on the SBF core that enhances the rigidity of the system and affects remarkably the crystal packing of **1** with respect to the fluorene analogous. Finally, the triplet state seems to be slightly affected by the presence of the spiro core, as can be deduced by the values obtained experimentally in PMMA thin films (Figure S15). The photophysical properties of **1** and **2** are summarized in Table 1.

DFT Calculations

To further investigate the electronic states and photophysical properties of **1** and **2**, DFT and TDDFT calculations were performed in toluene (see Supporting Information for Computational Details) employing the BMK hybrid exchange-correlation functional whose exchange part has a 42% contribution from Hartree-Fock exchange. This functional was previously found to perform well for TADF compounds, its Hartree-Fock percentage lying close to optimized values.[24] Compared to other popular functionals, we found that BMK also yields the most accurate prediction of emission wavelengths (see Table S3). The S_1 and T_1 states of both chromophores have a pronounced charge transfer character, with their frontier molecular orbitals being spatially completely separated and orthogonal. As depicted in Figure 4, the HOMO is mainly centered on the phenothiazine unit in both dyes, while the LUMO is localized on the cyanofluorene rest, underlying the little overlap between the two orbitals, which is essential characteristics to observe TADF. The HOMO/LUMO energy levels of **1** and **2** at the optimized ground state geometry are −5.91 eV/−1.25 eV and −5.91 eV/

Table 1. Photophysical properties of **1** and **2**.

Dye		λ_{exc} nm	λ_{em} nm	τ	PLQY %	ΔE_{ST} [e] eV	HOMO [f] eV	LUMO [f] eV
1	Toluene	296, 309, 326, 350	515	2.77 ns [a] 2.97 ns [b]		0.13	−5.91	−1.25
	Thin film	296, 327, 355	510	797.43 μs [c] 5.5 ns [d]	8.83			
	Crystal	350	462	248.64 μs [c] 1.95 ns [d]				
2	Toluene	292, 302, 314, 350	502	1.24 ns [a] 2.24 ns [b]		0.18	−5.91	−1.22
	Thin film	289, 313, 345	488	712.23 μs [c] 4.5 ns [d]	4.02			
	Crystal	418	470	153.34 μs [c] 1.67 ns [d]				

[a] oxygen containing solution ($1.5 \cdot 10^{-5}$ M and $7 \cdot 10^{-6}$ M for **1** and **2**, respectively), [b] deoxygenated solution ($1.5 \cdot 10^{-5}$ M and $7 \cdot 10^{-6}$ M for **1** and **2**, respectively), [c] delayed fluorescence lifetime (average value, see Supporting Information for multiexponential fit), [d] prompt fluorescence lifetime, [e] calculated using the quantum chemistry package Gaussian 09 Rev. D.01 with geometry optimization for the S_1 singlet exited state and the first triplet exited state T_1 geometry using the Tamm-Dancoff approximation, [f] calculated using the quantum chemistry package Gaussian 09 Rev. D.01.[23]

© 2024 The Author(s). ChemPhotoChem published by Wiley-VCH GmbH

23670932, 0, Downloaded from https://chemistry-europe.onlinelibrary.wiley.com/doi/10.1002/cptc.202400235 by UniversitaDegli Studi Di Mila, Wiley Online Library on [06/12/2024]. See the Terms and Conditions (https://onlinelibrary.wiley.com/terms-and-conditions) on Wiley Online Library for rules of use; OA articles are governed by the applicable Creative Commons License

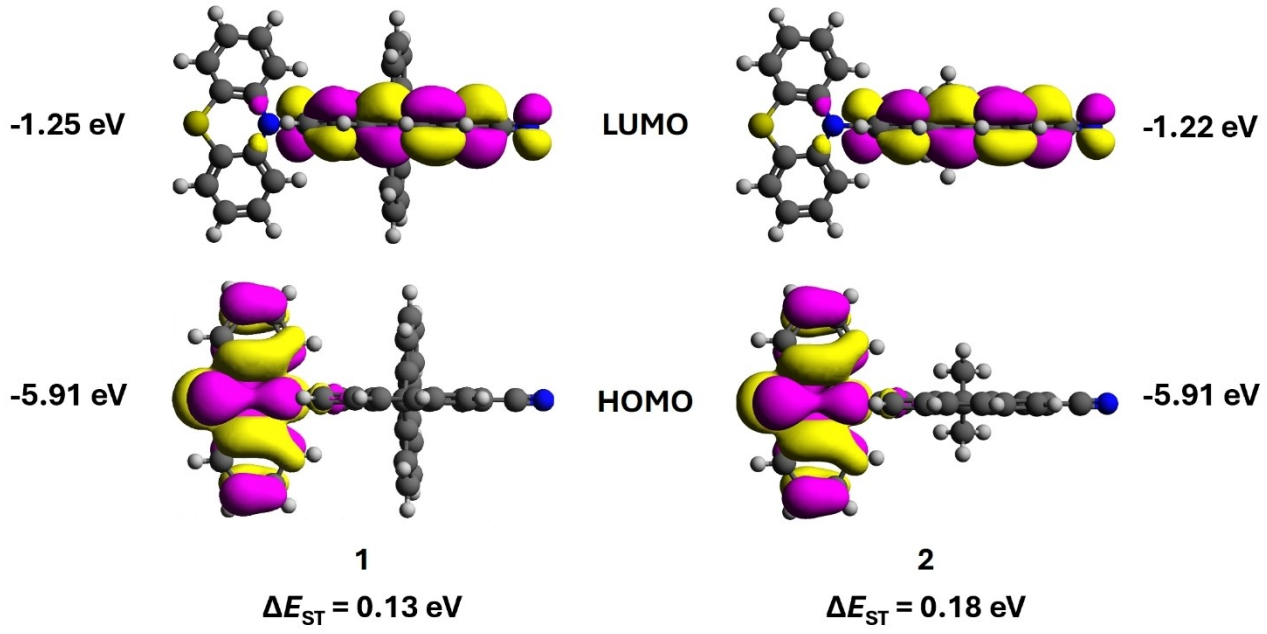

Figure 4. Calculated energy levels of **1** and **2** and the plotted orbitals of the HOMO and LUMO.

−1.22 eV, whereas their singlet-triplet splitting ΔE_{ST} obtained from the optimized S_1 and T_1 structures are 0.13 eV and 0.18 eV, respectively (Table 1). These values for the singlet-triplet splitting are low enough to facilitate RISC and allow TADF.[1c,7,25] The small difference in the HOMO/LUMO energy levels explain the similar emission behavior of the chromophores and the relatively high ΔE_{ST} might be the reason for the low PLQY. Although the triplet energy of the dyes has been estimated from the phosphorescence spectra in PMMA at 78 K (2.64 eV and 2.62 eV for **1** and **2**, respectively, Figure S15 and Table S4), the energy gaps calculated from experimental data appear larger than those obtained computationally. The emission band arising from the quasi-axial conformer of the phenothiazine unit band introduces a large error on the experimental data in both dyes, resulting in the overestimation of ΔE_{ST} (Figure S16 and Table S4).

X-Ray Analysis

The X-ray analysis of single crystals (Figures 5 and S18–S21) shows that the quasi-equatorial conformer is predominant in both chromophores, which is in accordance with the PL spectra where no or negligible emission around 400 nm is occurring. The emission for **2** in that range (Figure S13c) can therefore be explained by residual amount of the quasi-axial conformer, that might have deposited onto the crystals, after taking them out of the solution. The crystal structure of **1** reveals that a dimeric type structure is formed between two molecules. The molecules are arranged in line with a head-to-head and tail-to-tail configuration, so that the phenothiazine units are stacked upon each other due to strong π–π interactions with an interplane distance of 3.79 Å (the shortest distance is 3.43 Å between C55 and C65 atoms). Additional hydrogen bond interactions between these dimeric units involving two neighboring nitrile groups (C19–H19···N1 2.526 Å; 147°) contribute to the formation of a linear chain along the *bc*-diagonal with molecules in a head-to-head and tail-to-tail arrangement. CH-π interactions of

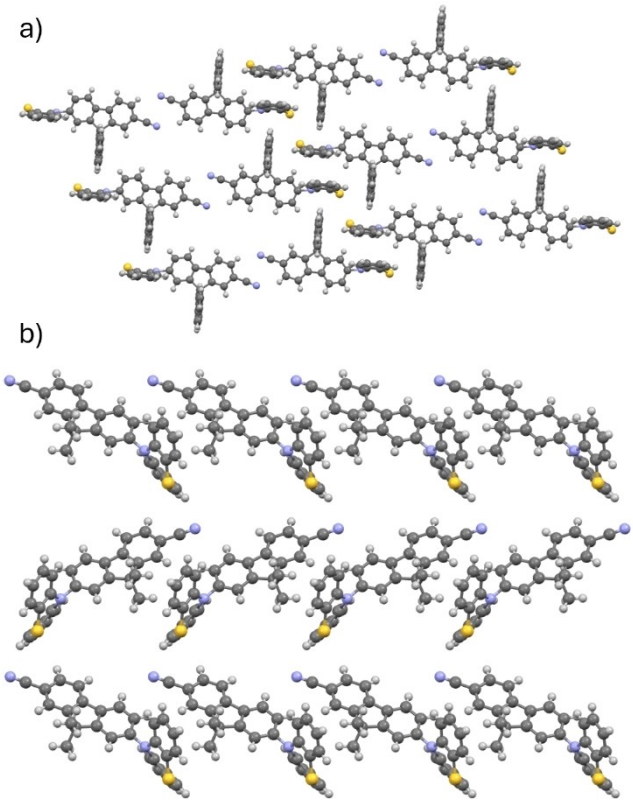

Figure 5. Crystal packing structure of **1** (a) and **2** (b).

© 2024 The Author(s). ChemPhotoChem published by Wiley-VCH GmbH

23670932, 0, Downloaded from https://chemistry-europe.onlinelibrary.wiley.com/doi/10.1002/cptc.202400235 by Universita'Degli Studi Di Mila , Wiley Online Library on [06/12/2024]. See the Terms and Conditions (https://onlinelibrary.wiley.com/terms-and-conditions) on Wiley Online Library for rules of use; OA articles are governed by the applicable Creative Commons License

the phenothiazine unit and the unsubstituted biphenyl moiety led to an inversion of the orientation of the adjacent molecule, resulting in a stair-like progression of the structure. The twist of the phenothiazine unit to the plane of the biphenyl unit is 82.6° contributing to the separation of the HOMO and LUMO (Figure S18).The crystal structure of **2** shows that the molecules are aligned with a head-to-tail orientation forming linear chains along the *b*-axis trough C–H···CN hydrogen bond interactions between the fluorene-core and phenothiazine (C15–H15···N1 2.60 Å; 125° and C14–H14···C23 2.90 Å; 135°). These interactions are supported by additional CH-π interactions between the methyl-groups and the neighboring phenothiazine unit (C31-H31B···C42 2.82 Å; 135° and C32-H32B···C54 2.97 Å; 137°). In contrast to spiro compound **1**, no π–π interactions between the phenothiazine units were observed. The adjacent biphenyl units are involved in the formation of weak π–π interactions with an interplanar distance of 3.87 Å. These have an inverted orientation due to the steric hinderance of the two methyl groups and favors the formation of the C–H···N hydrogen bond interactions between the nitrile group and the phenothiazine (C46–H46···N1 2.67 Å; 135°). The twist of the phenothiazine group with respect to the plane of the biphenyl unit is 79.3° (Figure S20). The X-ray structures of both dyes confirm the presence of a large dihedral angle between D and A groups necessary to minimize the HOMO/LUMO overlap. Moreover, the analysis of the crystalline form of **1** emphasizes the occurrence of intermolecular π–π interactions mainly between phenothiazine units, thus reducing the possibility of intermolecular CT interactions. The bulky spiro group hinders the π-stacking between D–A moieties, preventing the formation of emission quenching dimers.[26] In contrast, the methyl groups on the fluorene core of **2** do not offer the same steric hindrance, consequently intermolecular π–π interactions can affect the emissive behavior, resulting in smaller blueshift in regard to the PMMA thin film and shorter lifetime.[27] Nonetheless, both the spiro group and methyl groups of **1** and **2** contribute to the molecular separation in the crystalline phase, which leads to large blueshifted emission compared to solution or thin films, often observed in isolated molecules.[27]

Thermal Stability

Besides the photophysical properties, thermal stability properties of the dyes have been investigated by differential scanning calorimetry (DSC) and thermalgravimetric analysis (TGA) under nitrogen atmosphere (Figure S17). **1** and **2** show a fairly similar decomposition temperature (T_d, corresponding to a 5% weight loss) of 313.8 °C and 301.2 °C, respectively. The more rigid structure of the SBF core provides only a slight increase to T_d since the thermal stability of the phenothiazine unit is a limiting factor.[28] The DSC data shows that **1** doesn't melt and remains amorphous in the tested temperature range, while **2** melts at 187.8 °C. A crystallization could not be observed.

Conclusions

In conclusion, two novel TADF emitters (**1** and **2**) based on fluorene and spirobifluorene core were synthesized and their physical properties investigated with regard to emission and thermal behavior. In solution, both dyes behaved similarly without showing TADF behavior. On the contrary, long delayed fluorescence component were detected in doped PMMA thin films and crystals and assigned to TADF process through lifetime measurements at different temperatures. Very interestingly, **2** is the first fluorenecarbonitrile derivative showing TADF. By comparing the two dyes, we can conclude that the SBF-linker leads small bathochromic shift of the emission as effect of the spiro-conjugation, an increase in the fluorescence lifetime and in the PLQY, as well as a better thermal stability. Moreover, the bulky spiro-core plays a role on the intermolecular interactions, reducing the presence of additional non radiative deactivation pathways such as the π–π packing. Our study stresses the importance of proper selection of conjugated spacer and demonstrates that the structural alterations of molecular core may have evident effects to emission properties.

Supporting Information Summary

The authors have cited additional references within the Supporting Information.[18,22,24,29]

Deposition numbers CCDC-2355946 (for compound **1**) and −2355947 (for compound **2**) contain the supplementary crystallographic data for this paper. These data are provided free of charge by the joint Cambridge Crystallographic Data Centre and Fachinformationszentrum Karlsruhe Access Structures service www.ccdc.cam.ac.uk/structures.

Acknowledgements

The authors thank Debbie Stappers for measuring DSC and TGA. FR thanks the Deutsche Forschungsgemeinschaft (DFG) (grant number RI 2635/6-1, project number: 464509280) for funding. Open Access funding enabled and organized by Projekt DEAL.

Conflict of Interests

The authors declare no conflict of interest.

Data Availability Statement

The data that support the findings of this study are available from the corresponding author upon reasonable request.

Keywords: Delayed fluorescence · Spirobifluorene · Fluorene · Fluorescence · Phenothiazine

© 2024 The Author(s). ChemPhotoChem published by Wiley-VCH GmbH

23670932, 0, Downloaded from https://chemistry-europe.onlinelibrary.wiley.com/doi/10.1002/cptc.202400235 by UniversitaDegli Studi Di Mila, Wiley Online Library on [06/12/2024]. See the Terms and Conditions (https://onlinelibrary.wiley.com/terms-and-conditions) on Wiley Online Library for rules of use; OA articles are governed by the applicable Creative Commons License

[1] a) Y. Tao, K. Yuan, T. Chen, P. Xu, H. Li, R. Chen, C. Zheng, L. Zhang, W. Huang, *Adv. Mater.* **2014**, *26*, 7931–7958; b) C. W. Tang, S. A. VanSlyke, *Apl. Phys. Lett.* **1987**, *51*, 913–915; c) H. Uoyama, K. Goushi, K. Shizu, H. Nomura, C. Adachi, *Nature* **2012**, *492*, 234–238; d) H. Nakanotani, T. Higuchi, T. Furukawa, K. Masui, K. Morimoto, M. Numata, H. Tanaka, Y. Sagara, T. Yasuda, C. Adachi, *Nat. Commun.* **2014**, *5*, 4016; e) F. Rizzo, F. Cucinotta, *Isr. J. Chem.* **2018**, *58*, 874–888.

[2] a) J. You, L. Dou, K. Yoshimura, T. Kato, K. Ohya, T. Moriarty, K. Emery, C.-C. Chen, J. Gao, G. Li, Y. Yang, *Nat. Commun.* **2013**, *4*, 1446; b) H. J. Son, L. Lu, W. Chen, T. Xu, T. Zheng, B. Carsten, J. Strzalka, S. B. Darling, L. X. Chen, L. Yu, *Adv. Mater.* **2013**, *25*, 838–843.

[3] a) X. Xiong, F. Song, J. Wang, Y. Zhang, Y. Xue, L. Sun, N. Jiang, P. Gao, L. Tian, X. Peng, *J. Am. Chem. Soc.* **2014**, *136*, 9590–9597; b) L. E. Kreno, K. Leong, O. K. Farha, M. Allendorf, R. P. van Duyne, J. T. Hupp, *Chem. Rev.* **2012**, *112*, 1105–1125; c) M. Vendrell, D. Zhai, J. C. Er, Y.-T. Chang, *Chem. Rev.* **2012**, *112*, 4391–4420.

[4] M. A. Bryden, E. Zysman-Colman, *Chem. Soc. Rev.* **2021**, *50*, 7587–7680.

[5] a) F. B. Dias, K. N. Bourdakos, V. Jankus, K. C. Moss, K. T. Kamtekar, V. Bhalla, J. Santos, M. R. Bryce, A. P. Monkman, *Adv. Mater.* **2013**, *25*, 3707–3714; b) V. Jankus, P. Data, D. Graves, C. McGuinness, J. Santos, M. R. Bryce, F. B. Dias, A. P. Monkman, *Adv. Funct. Mater.* **2014**, *24*, 6178–6186; c) P. L. Santos, J. S. Ward, P. Data, A. S. Batsanov, M. R. Bryce, F. B. Dias, A. P. Monkman, *J. Mater. Chem. C* **2016**, *4*, 3815–3824.

[6] a) M. Y. Wong, E. Zysman-Colman, *Adv. Mater.* **2017**, *29*, 1605444; b) T. Hatakeyama, K. Shiren, K. Nakajima, S. Nomura, S. Nakatsuka, K. Kinoshita, J. Ni, Y. Ono, T. Ikuta, *Adv. Mater.* **2016**, *28*, 2777–2781; c) H. Noda, H. Nakanotani, C. Adachi, *Sci. Adv.* **2018**, *4*, eaao6910.

[7] T. Nakagawa, S.-Y. Ku, K.-T. Wong, C. Adachi, *Chem. Comm.* **2012**, *48*, 9580–9582.

[8] a) H. Tsujimoto, D.-G. Ha, G. Markopoulos, H. S. Chae, M. A. Baldo, T. M. Swager, *J. Am. Chem. Soc.* **2017**, *139*, 4894–4900; b) G. Méhes, H. Nomura, Q. Zhang, T. Nakagawa, C. Adachi, *Angew. Chem, Int. Ed.* **2012**, *51*, 11311–11315.

[9] a) H. Wang, J.-X. Chen, X. Zhang, Y.-C. Cheng, X.-C. Fan, L. Zhou, J. Yu, K. Wang, X.-H. Zhang, *Adv. Opt. Mater.* **2023**, *11*, 2300368; b) W. Li, B. Li, X. Cai, L. Gan, Z. Xu, W. Li, K. Liu, D. Chen, S.-J. Su, *Angew. Chem, Int. Ed.* **2019**, *58*, 11301–11305; c) H. Liu, H. Liu, J. Fan, J. Guo, J. Zeng, F. Qiu, Z. Zhao, B. Z. Tang, *Adv. Opt. Mater.* **2020**, *8*, 2001027; d) J.-F. Liu, X.-Q. Wang, Y.-J. Yu, S.-N. Zou, S.-Y. Yang, Z.-Q. Jiang, L.-S. Liao, *Org. Electron.* **2021**, *91*, 106088.

[10] a) Z. Zhang, G. Zhao, H. Chen, T. Zhou, W. Tian, W. Jiang, Y. Sun, *Org. Electron.* **2024**, *128*, 107043; b) A. Gil-Martínez, S. López-Molina, C. Galiana-Roselló, A. Lázaro-Gómez, F. Schlüter, F. Rizzo, J. González-García, *Chem. Eur. J.* **2023**, *29*, e202203094; c) T. Matsumoto, T. Murakami, F. Schlüter, H. Murata, V. Vohra, F. Rizzo, *Solar RRL* **2022**, *6*, 2100661; d) F. Schlüter, B. J. Ravoo, F. Rizzo, *J. Mater. Chem. B* **2019**, *7*, 4933–4939; e) G. Bottaro, F. Rizzo, M. Cavazzini, L. Armelao, S. Quici, *Chem. Eur. J.* **2014**, *20*, 4598–4607; f) K. Okubo, K. Oka, K. Tsuchiya, A. Tomimoto, N. Tohnai, *Angew. Chem, Int. Ed.* **2024**, *63*, e202400475; g) L. Sicard, C. Brouillac, N. Leclerc, S. Fall, N. Zimmerman, O. Jeannin, J. Rault-Berthelot, C. Quinton, C. Poriel, *Mater. Chem. Front.* **2024**, *8*, 1349–1361.

[11] a) T. P. I. Saragi, T. Spehr, A. Siebert, T. Fuhrmann-Lieker, J. Salbeck, *Chem. Rev.* **2007**, *107*, 1011–1065; b) T. P. I. Saragi, T. Fuhrmann-Lieker, J. Salbeck, *Adv. Funct. Mater.* **2006**, *16*, 966–974.

[12] a) X. Tang, L.-S. Cui, H.-C. Li, A. J. Gillett, F. Auras, Y.-K. Qu, C. Zhong, S. T. E. Jones, Z.-Q. Jiang, R. H. Friend, L.-S. Liao, *Nat. Mater.* **2020**, *19*, 1332–1338; b) C.-C. Peng, S.-Y. Yang, H.-C. Li, G.-H. Xie, L.-S. Cui, S.-N. Zou, C. Poriel, Z.-Q. Jiang, L.-S. Liao, *Adv. Mater.* **2020**, *32*, e2003885.

[13] a) X. Tian, M. Yao, X. Liang, C. Zhou, S. Xiao, Y. Gao, H. Liu, S.-T. Zhang, B. Yang, *Dyes Pigm.* **2022**, *205*, 110463; b) T. Serevičius, R. Skaisgiris, D. Banevičius, S. Tumkevičius, J. Dodonova-Vaitkūnienė, S. Juršėnas, *Dyes Pigm.* **2023**, *220*, 111711.

[14] A. U. Neelambra, C. Govind, T. T. Devassia, G. M. Somashekharappa, V. Karunakaran, *Phys. Chem. Chem. Phys.* **2019**, *21*, 11087–11102.

[15] X. Liu, W. Liu, W. Dongyu, X. Wei, L. Wang, H. Wang, Y. Miao, H. Xu, J. Yu, B. Xu, *J. Mater. Chem. C* **2020**, *8*, 14117–14124.

[16] X. Qiu, S. Ying, C. Wang, M. Hanif, Y. Xu, Y. Li, R. Zhao, D. Hu, D. Ma, Y. Ma, *J. Mater. Chem. C* **2019**, *7*, 592–600.

[17] a) F. Polo, F. Rizzo, M. Veiga-Gutierrez, L. de Cola, S. Quici, *J. Am. Chem. Soc.* **2012**, *134*, 15402–15409; b) F. Rizzo, F. Polo, G. Bottaro, S. Fantacci, S. Antonello, L. Armelao, S. Quici, F. Maran, *J. Am. Chem. Soc.* **2017**, *139*, 2060–2069.

[18] W. Wang, X. Yang, R. Dai, Z. Yan, J. Wei, X. Dou, X. Qiu, H. Zhang, C. Wang, Y. Liu, S. Song, N. Jiao, *J. Am. Chem. Soc.* **2022**, *144*, 13415–13425.

[19] a) I. Marghad, F. Bencheikh, C. Wang, S. Manolikakes, A. Rérat, C. Gosmini, D. H. Kim, J.-C. Ribierre, C. Adachi, *RSC Adv.* **2019**, *9*, 4336–4343; b) I. Marghad, D. H. Kim, X. Tian, F. Mathevet, C. Gosmini, J.-C. Ribierre, C. Adachi, *ACS Omega* **2018**, *3*, 2254–2260; c) M. Okazaki, Y. Takeda, P. Data, P. Pander, H. Higginbotham, A. P. Monkman, S. Minakata, *Chem. Sci.* **2017**, *8*, 2677–2686; d) H. Tanaka, K. Shizu, H. Nakanotani, C. Adachi, *J. Phys. Chem. C* **2014**, *118*, 15985–15994.

[20] a) K. J. Lee, Y. U. Lee, F. Fages, J.-C. Ribierre, J. W. Wu, A. D'Aléo, *Nano Lett.* **2018**, *18*, 1476–1482; b) I. Renge, *Chem. Phys. Lett.* **2003**, *377*, 286–292.

[21] L. Vaghi, F. Rizzo, *Solar RRL* **2023**, *7*, 2201108.

[22] A. Yadigarli, Q. Song, S. I. Druzhinin, H. Schönherr, *Beilstein J. Org. Chem.* **2019**, *15*, 2552–2562.

[23] M. J. Frisch, G. W. Trucks, H. B. Schlegel, G. E. Scuseria, M. A. Robb, J. R. Cheeseman, G. Scalmani, V. Barone, B. Mennucci, Petersson et al. *Gaussian 09*, Gaussian Inc, Wallingford CT **2013**.

[24] a) Q. Zhang, H. Kuwabara, W. J. Potscavage, S. Huang, Y. Hatae, T. Shibata, C. Adachi, *J. Am. Chem. Soc.* **2014**, *136*, 18070–18081; b) S. Huang, Q. Zhang, Y. Shiota, T. Nakagawa, K. Kuwabara, K. Yoshizawa, C. Adachi, *JTCC* **2013**, *9*, 3872–3877.

[25] B. Valeur, *Molecular Fluorescence: Principles And Applications*, Wiley-VCH, Weinheim, **2009**.

[26] a) M. K. Etherington, N. A. Kukhta, H. F. Higginbotham, A. Danos, A. N. Bismillah, D. R. Graves, P. R. McGonigal, N. Haase, A. Morherr, A. S. Batsanov, C. Pflumm, V. Bhalla, M. R. Bryce, A. P. Monkman, *J. Phys. Chem. C* **2019**, *123*, 11109–11117; b) H. Langhals, R. Ismael, O. Yürük, *Tetrahedron* **2000**, *56*, 5435–5441; c) T. Meier, H. Bässler, A. Köhler, *Adv. Opt. Mater.* **2021**, *9*, 2100115.

[27] A. Maggiore, X. Tan, A. Brosseau, A. Danos, F. Miomandre, A. P. Monkman, P. Audebert, G. Clavier, *Phys. Chem. Chem. Phys.* **2022**, *24*, 17770–17781.

[28] X. Liang, C. Wang, M. Wu, Y. Wu, F. Zhang, Z. Han, X. Lu, K. Guo, Y.-M. Zhao, *Tetrahedron* **2017**, *73*, 7115–7121.

[29] a) J. Tomasi, B. Mennucci, R. Cammi, *Chem. Rev.* **2005**, *105*, 2999–3093; b) A. K. Rappe, C. J. Casewit, K. S. Colwell, W. A. Goddard, W. M. Skiff, *J. Am. Chem. Soc.* **1992**, *114*, 10024–10035; c) A. D. Boese, J. M. L. Martin, *J. Chem. Phys.* **2004**, *121*, 3405–3416; d) A. D. Becke, *J. Chem. Phys.* **1993**, *98*, 5648–5652; e) C. Adamo, V. Barone, *J. Chem. Phys.* **1999**, *110*, 6158–6170; f) Y. Zhao, D. G. Truhlar, *Theor. Chem. Acc.* **2008**, *120*, 215–241; g) M. D. Hanwell, D. E. Curtis, D. C. Lonie, T. Vandermeersch, E. Zurek, G. R. Hutchison, *J. Cheminform.* **2012**, *4*, 17; h) Bruker AXS, *APEX4*, **2021**; i) G. M. Sheldrick, *Acta Cryst.* **2015**, *71*, 3–8; j) G. M. Sheldrick, *Acta Cryst.* **2015**, *71*, 3–8; k) Bruker AXS, Interactive Molecular Graphics Bruker AXS, Madison, Wisconsin, USA **1998**; l) B. A. Anderson, E. C. Bell, F. O. Ginah, N. K. Harn, L. M. Pagh, J. P. Wepsiec, *J. Org. Chem.* **1998**, *63*, 8224–8228; m) M. Nishiyama, T. Yamamoto, Y. Koie, *Tetrahedron Lett.* **1998**, *39*, 617–620.

Manuscript received: June 24, 2024
Revised manuscript received: September 9, 2024
Accepted manuscript online: September 12, 2024
Version of record online: ■■, ■■

© 2024 The Author(s). ChemPhotoChem published by Wiley-VCH GmbH

23670932, 0, Downloaded from https://chemistry-europe.onlinelibrary.wiley.com/doi/10.1002/cptc.202400235 by UniversitaDegli Studi Di Mila, Wiley Online Library on [06/12/2024]. See the Terms and Conditions (https://onlinelibrary.wiley.com/terms-and-conditions) on Wiley Online Library for rules of use; OA articles are governed by the applicable Creative Commons License

RESEARCH ARTICLE

The properties of TADF emitters are highly dependent on the chosen electron donor and acceptor, as well as the π-system that links them together. Herein, we show that another π-system attached to the linker has an influence on the emissive behavior of fluorene-based systems.

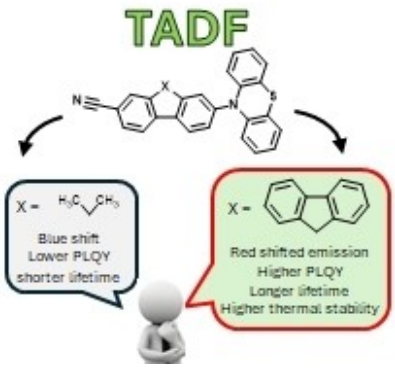

*T. Silies, N. L. Doltsinis, C. G. Daniliuc, F. Rizzo**

1 – 8

Fluorene vs. Spirobifluorene: Effect of the π-System on TADF Properties

23670932, 0, Downloaded from https://chemistry-europe.onlinelibrary.wiley.com/doi/10.1002/cptc.202400235 by UniversitaDegli Studi Di Mila, Wiley Online Library on [06/12/2024]. See the Terms and Conditions (https://onlinelibrary.wiley.com/terms-and-conditions) on Wiley Online Library for rules of use; OA articles are governed by the applicable Creative Commons License